



Development of the BioBattery: A novel enzyme fuel cell using a multicopper oxidase as an anodic enzyme

Kartheek Batchu^{a,1}, David Probst^{a,1}, Takenori Satomura^b, Koji Sode^{a,*}

^a Joint Department of Biomedical Engineering, University of North Carolina at Chapel Hill and North Carolina State University, Chapel Hill, NC, 27599, USA

^b Division of Engineering, Faculty of Engineering, University of Fukui, Fukui, Japan

ARTICLE INFO

Keywords:

Enzyme fuel cell
Multicopper oxidase
BioBattery
BioCapacitor

ABSTRACT

This work presents the development of an enzyme fuel cell, termed “BioBattery”, that utilizes multicopper oxidases as the anodic enzyme in a non-diffusion limited system. We evaluated various enzyme variants as the anode, including multicopper oxidase from *Pyrobaculum aerophilum*, laccase from *Trametes versicolor*, and bilirubin oxidase from *Myrothecium verrucaria*. Several combinations of cathodes were also examined, focusing on the reduction of oxygen as the primary electron acceptor. The optimal pairing used multicopper oxidase from *Pyrobaculum aerophilum* as the anode and amine reactive phenazine ethosulfate modified bovine serum albumin as the cathode. BioBattery was integrated with our previously developed BioCapacitor, proving capable of consistently powering a 470 μ F capacitor, positioning it as a modular power source for wearable and implantable systems. This research work addresses and overcomes some of the fundamental limitations seen in enzyme fuel cells, where power and current are often limited by substrate accessibility to the active electrode surface. (152 words).

1. Introduction

Over recent decades, enzyme cells have garnered significant attention, crossing paths with diverse fields such as green energy, nanotechnology, electrochemistry, material science, and beyond (Heller, 2004; Kumar et al., 2018; Sharma et al., 2021; Xiao et al., 2019). These systems have found applications in wearable sensors, textiles, and even environmental setups, leveraging a range of fuels—from naturally occurring sugars in implantable systems to wastewater in treatment facilities (Jeeranpan et al., 2020). However, despite their broad applications and versatility, enzyme fuel cells face significant hurdles in areas like stability, power output, and miniaturization potential. Recent achievements in enzyme fuel cells showed high power density but suffer from compromised stability, with performance deteriorating after sustained use (A. Karim et al., 2021; Calabrese Barton et al., 2004; Slate et al., 2019; Xiao et al., 2019). Notably, the enzyme fuel systems offer notable advantages over traditional power sources, operating effectively in physiological conditions, catalyzing reactions at body temperature and pH, and mitigating many of the waste issues associated with conventional power systems.

One of the core limitations for many enzyme fuel cells is the need for

fuel to diffuse from a bulk solution into the anode’s active region. This is a notable distinction from the conventionally utilized “coin batteries” embedded in several medical devices. This diffusion places inherent constraints on in vivo power density due to several factors. Firstly, typical physiological fuels are present in low concentrations in vivo, with glucose ranging from 4 to 7 mM, lactate between 1 and 3 mM, and oxygen at about 0.1 mM (Gough et al., 1982; Heikenfeld et al., 2019; Pucino et al., 2017). Secondly, many enzyme fuel cells that depend on their substrates encounter mass transport limitations, meaning their peak current or power output is restricted by the rate at which substrates diffuse from the bulk solution. Once implanted, this diffusion can be further inhibited by the body’s foreign response, potentially encapsulating the device. Additionally, the voltage differences across enzymatic fuel cells are often much lower than the requirements of most contemporary microsystem electronics, typically staying below 700 mV due to ohmic losses across the system, whereas many microprocessors require between 0.8 and 1.2 V (Barelli et al., 2021; Harris, 2007). To address these challenges, several groups have employed strategies such as nanotechnology to amplify effective surface area or by placing the fuel cell in a location with sufficient convection to greatly enhance the mass limited power. While these solutions enhance power output and

* Corresponding author.

E-mail address: ksode@email.unc.edu (K. Sode).

¹ These authors contributed equally to this work.

applicability, they either confine the cell to specific scenarios (like implanting it within an artery or vein) or pose complications for miniaturization. Ideally the enzymatic biofuel cell would have the substrate built into the system, enabling non-diffusion limited power, as well as making miniaturization, and integration less burdensome, as this would resemble the form factor of modern coin cells.

This article introduces a design for enzyme fuel cells that embeds fuel within the anode materials, a concept we have designated as ‘Bio-Battery’. As shown in Fig. 1, the substrate is co-immobilized with the enzyme, allowing for sufficient power generation, eliminating the dependence on the bulk mass transfer of a specific fuel by having no outer membrane. This proposed system also maintaining both biocompatibility and environmental friendliness. The anode is functionalized by immobilizing a hyper-thermostable multicopper oxidase, specifically one derived from the hyper-thermophilic archaeon *Pyrobaculum aerophilum* (McoP) (Sakuraba et al., 2011), onto carbon paper using glutaraldehyde. It has been well established that during the cross-linking of glutaraldehyde, the reaction often polymerizes, producing varieties of complex structures, including polyphenolic compounds (Migneault et al., 2004). We serendipitously found that McoP can oxidize cross-linked glutaraldehyde, acting as a “fuel”, and can generate electricity when it is combined with cathodic materials harboring oxygen-sensitive redox-compounds, such as phenazine ethosulfate (PES). The cathode is, therefore, functionalized by the immobilization of bovine serum albumin (BSA) modified with amine-reactive PES (arPES-BSA). This enzymatic biofuel cell is then paired with our previously developed BioCapacitor, which our group has used to power glucose sensors, microprocessors, and step motors (Hanashi et al., 2011; Lee et al., 2021; Sode et al., 2016). We assessed this system using a variety of multicopper enzymes and paired it with various cathodes to gauge the resultant power and current output.

2. Methods

2.1. Reagents and materials

In this study, several multicopper oxidases were utilized: multicopper oxidase from *Pyrobaculum aerophilum* (McoP), laccase from *Trametes versicolor*, and bilirubin oxidase (BOD) from *Myrothecium verrucaria*. McoP was recombinantly produced using the expression vector pET-11a-pae1888 and purified as previously described (Satomura et al., 2021). The vectors were transformed into *Escherichia coli* strain BL21-CodonPlus (DE3)-RIPL and cultivated as previously described. Laccase from *T. versicolor*, BOD from *M. verrucaria*, and bovine serum albumin (BSA) were purchased from MilliporeSigma (Burlington, MA,

USA). Gold disk electrodes (GDE) were purchased from BAS Inc. (Tokyo, Japan). arPES was purchased from Dojindo Molecular Technology, Inc. (Rockville, MD, USA). Toray carbon paper (TCP) was purchased from FuelCellEarth (Woburn, Massachusetts, USA). Glutaraldehyde, 25% aqueous solution and Triton X-100 was purchased from MilliporeSigma (Burlington, MA, USA). Ketjen black (KB) powder was purchased from Mitsubishi Chemical Corp. (Tokyo, Japan). The ADP5090 Ultralow Power Boost Regulator with MPPT and Charge Management circuit was purchased from Analog Devices (Wilmington, MA, USA). The Eisco 6 Decade Resistance Box was purchased from Amazon. All electrochemical measurements were performed on the VSP-3e Potentiostat from BioLogic.

2.2. Preparation of McoP: recombinant expression and purification

McoP was prepared as previously described (Satomura et al., 2021). Recombinant production was performed using the expression vector pET-11a-pae1888 plasmid. These vectors were transformed into *E. coli* BL21-CodonPlus (DE3)-RIPL. The transformed *E. coli* were cultured in 200 mL conical flasks on a rotary shaker at 37 °C for 30 h. Cells were subsequently harvested via centrifugation. The collected wet cells were disrupted through ultrasonication in 10 mM Tris-HCl buffer with a pH of 7.2. The lysate was centrifuged at 12,000 rpm for 15 min and then incubated in 1 mM copper sulfate for 16 h. After this, the enzyme solution was heated to 80 °C for 10 min. The enzyme medium was then exchanged for 10 mM Tris-HCl buffer (pH 8.0).

2.3. Preparation of KB ink

The KB ink was prepared by combining 15 mg of KB powder with 670 μ L of Milli-Q water and 30 μ L of Triton X-100. The resulting mixture was sonicated for a duration of 1 h and subsequently stored in a dark environment. Prior to each application, the solution underwent re-sonication for an additional 30 min to ensure a homogeneous ink formulation.

2.4. arPES conjugation

For the modification of BSA with arPES, a mixture was prepared using the following reagents: 140 μ L of 50 mg/mL BSA, 100 μ L of 100 mM potassium phosphate buffer (PPB) buffer, and 10 μ L of 50 mM arPES. This mixture was subjected to shaking at 1200 rpm for 30 min at a temperature of 4 °C to facilitate conjugation. Afterwards, a buffer exchange was performed via centrifugation under the conditions of 14,000 g, 4 °C, and a 5-min duration; this step was repeated 10 times.

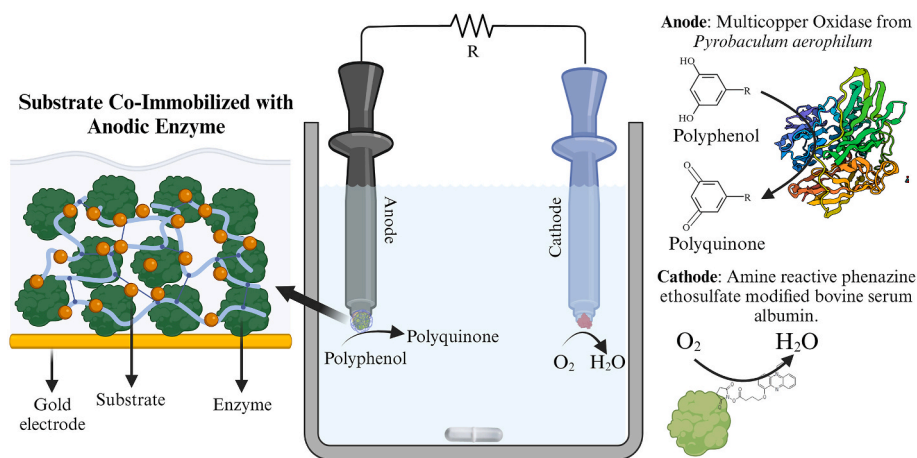


Fig. 1. An overview of the proposed BioBattery design. The anode utilizes a multicopper oxidase from *Pyrobaculum aerophilum*, oxidizing polyphenols to polyquinones. Concurrently, the cathode employs an amine reactive phenazine ethosulfate modified bovine serum albumin, facilitating the reduction of O₂ to H₂O. Notably, the substrate is co-immobilized with the anodic enzyme, thereby dramatically reducing substrate transport diffusion limitations.

2.5. Preparation of enzyme mixes

For the anodes, the following enzyme inks were mixed: McoP (10 μ L of 40 mg/ml McoP, 3 μ L of KB ink, and 17 μ L of PPB), BOD (10 μ L of 5.4 mg/ml BOD, 3 μ L of KB ink, and 17 μ L of PPB), and Laccase (10 μ L of 40 mg/ml laccase, 3 μ L of KB ink, and 17 μ L of PPB). For the cathodes, the following enzyme inks were mixed: arPES-BSA (10 μ L of 50 mg/ml arPES-BSA, 3 μ L of KB ink, and 17 μ L of PPB), BOD (10 μ L of 5.4 mg/ml BOD, 3 μ L of KB ink, and 17 μ L of PPB), and Laccase (10 μ L of 40 mg/ml Laccase, 3 μ L of KB ink, and 17 μ L of PPB).

2.6. Preparation of GDE BioBattery

GDEs ($\Phi = 2$ mm) were polished using 0.3 and 0.05 μ m alumina powder, then washed with piranha (H_2SO_4 : 30%, $\text{H}_2\text{O}_2 = 3:1$) for 1 h. These electrodes were then subjected to electrochemical purification through cyclic voltammetry sweeps ranging from 0.0 V to 1.2 V in a 50 mM KOH solution. The resulting anode/cathode enzyme ink is subsequently dropcast onto the surface of the GDE. After this step, the electrode undergoes glutaraldehyde vapor deposition using a 25% glutaraldehyde solution, followed by incubation in 10 mM Tris-HCl for 20 min. The electrode is ultimately stored in 100 mM PPB until needed for use.

2.7. Preparation of TCP BioBattery

A section measuring approximately 1 inch by 1 inch is cut from a larger piece of TCP. This cut section is then sprayed with deionized water to cleanse its surface of any accumulated dirt or grime. Following this, the anode or cathode enzyme ink is dropcast onto the surface of the TCP. Following this, the electrode is subjected to vapor deposition using a 25% glutaraldehyde solution and then incubated in 10 mM Tris-HCl for a period of 20 min. Ultimately, the electrode is stored in 100 mM PPB until it is required for use.

2.8. Calculation of TCP electrode surface area

Anodic enzyme was immobilized onto TCP electrodes as detailed above. An image of the surface was then taken and uploaded into ImageJ, where the oval tool was used to determine the surface area of the enzyme spots. These were then averaged across 18 enzyme spots and used to calculate the associated power and current density of the biofuel cell (Supplemental Fig. S3).

2.9. BioBattery characterization

The selected anode and the cathode are positioned in a cell containing 100 mM PPB. Subsequently, they are connected to a potentiostat and a Decade Resistance Box to apply varying loads. During the measurement of the open-circuit potential (OCP), different resistances (200 Ω , 500 Ω , 800 Ω , 2000 Ω , 5000 Ω , 8000 Ω , 20,000 Ω , 50,000 Ω , 80,000 Ω , 200,000 Ω , 500,000 Ω , 800,000 Ω , and 1,000,000 Ω) are applied across the enzyme biofuel cell, and the resultant potential across the fuel cell is recorded. Utilizing the known resistance values (applied through the Eisco 6 Decade Resistance Box) and the potential values (obtained from the OCP measurements), the current flow and power output of the cell are calculated.

2.10. Application of BioBattery in power generation

The anode (TCP-McoP electrode) and the cathode (TCP-arPES-BSA electrode) are positioned in a cell containing 100 mM PPB, which are then connected to the ADP5090 charge pump circuit. To this circuit, a selected capacitor, either 47 μ F or 470 μ F, is connected. The potentiostat is attached to both leads of the capacitor, enabling the measurement of the open circuit potential.

3. Results and discussion

To validate the enzymatic biofuel cell, we investigated several different anodic enzymes (laccase from *T. versicolor*, BOD from *M. verrucaria*, and McoP from *P. aerophilum*) which can oxidize polyphenol groups into polyquinones (Supplemental Figs. S2 and S4) to drive current, along with several possible cathodic electrodes to optimize the power and current produced (BOD, laccase, and arPES – BSA mixed with ketjen black). Fig. 2 shows our proposed BioBattery system, emphasizing the effects of stacking in series and parallel configurations and the influence of increasing immobilized anodic layers. All electrochemical characterizations were conducted using gold disk electrodes (GDEs, $\Phi = 2$ mm). Fig. 2a and b illustrate the power and current densities of various anodic enzymes immobilized on GDEs. Of the three anodic enzymes tested for peak power and current outputs—laccase ($0.016 \text{ W/m}^2 \pm 0.006 \text{ W/m}^2$, $0.032 \text{ A/m}^2 \pm 0.008 \text{ A/m}^2$), BOD ($0.22 \text{ W/m}^2 \pm 0.03 \text{ W/m}^2$, $0.48 \text{ A/m}^2 \pm 0.04 \text{ A/m}^2$), and McoP ($0.45 \text{ W/m}^2 \pm 0.02 \text{ W/m}^2$, $0.56 \text{ A/m}^2 \pm 0.08 \text{ A/m}^2$)—McoP produced the highest power and current density in comparison to the others. All these anodes were assessed in conjunction with an arPES-BSA cathode. Fig. 2c and d presents the power and current outputs when using cathodes employing either BOD, arPES-BSA, or Laccase, each mixed with ketjen black, and paired with an McoP anodic electrode. Of the three cathodic enzymes tested for peak power and current densities—laccase ($0.057 \text{ W/m}^2 \pm 0.007 \text{ W/m}^2$, $0.058 \text{ A/m}^2 \pm 0.009 \text{ A/m}^2$), BOD ($0.13 \text{ W/m}^2 \pm 0.02 \text{ W/m}^2$, $0.38 \text{ A/m}^2 \pm 0.07 \text{ A/m}^2$), and arPES-BSA ($0.46 \text{ W/m}^2 \pm 0.03 \text{ W/m}^2$, $0.56 \text{ A/m}^2 \pm 0.05 \text{ A/m}^2$)—arPES-BSA produced the highest power and current density when paired with a McoP anode. Fig. 2e and f displays the power and current outputs across various anodic layers. Specifically, a 1-layer produced densities of ($0.25 \text{ W/m}^2 \pm 0.04 \text{ W/m}^2$ at 250 mV ± 42 mV, $0.18 \text{ A/m}^2 \pm 0.04 \text{ A/m}^2$), 2-layers produced ($0.23 \text{ W/m}^2 \pm 0.03 \text{ W/m}^2$ at 141 mV ± 34 mV, $0.16 \text{ A/m}^2 \pm 0.03 \text{ A/m}^2$), and 3-layers yielded ($0.28 \text{ W/m}^2 \pm 0.05 \text{ W/m}^2$ at 265 mV ± 34 mV, $0.19 \text{ A/m}^2 \pm 0.03 \text{ A/m}^2$). Notably, the minimal variations observed between the 1–3 anodic enzyme layers (GDE-McoP) suggest potential cathodic limitations of the system (GDE-arPES-BSA), influenced by surface area constraints. The curves represented reflect mean values derived from three individual GDE experiments ($n = 3$). Fig. 2g and h displays the power and current densities of configurations ranging from 1 to 3 cells. Specifically, Fig. 2g, denoting series configurations, is color-coded: red for 1 cell (0.27 W/m^2 , peak potential: 292 mV), green for 2 cells (0.52 W/m^2 , peak potential: 324 mV), and blue for 3 cells (0.91 W/m^2 , peak potential: 380 mV). This emphasizes the enhancement in potential difference as more cells are connected in series. Conversely, Fig. 2h, representing parallel configurations, follows the same color-coding—1 cell (0.30 A/m^2), 2 cells (0.64 A/m^2), and 3 cells (0.95 A/m^2)—highlighting the increase in peak current densities with more cells connected in parallel. Within this system, McoP serves as the anode, and arPES-BSA functions as the cathode. Evidently, increasing the number of cells in the biofuel system significantly improves both the potential difference (in series) and the current output (in parallel). Additionally, we further characterized the polarization behavior of our biofuel cell by measuring the open circuit potential of a GDE-McoP anode paired with a GDE-arPES-BSA cathode. This measurement showed no signal decay until approximately 3200 s (Supplemental Fig. S1).

From the results in Fig. 2, we opted for the biofuel cell configuration utilizing McoP as the anodic electrode and arPES-BSA for the cathodic electrode. McoP demonstrated a superior response (Fig. 2) using glutaraldehyde. McoP was originally derived from extremophile (Sakuraba et al., 2011), and then engineered (Satomura et al., 2021) to improve its catalytic activity without losing its hyper-thermostability. The original enzyme has already been demonstrated to be stable in biofuel cell format and the stability of the electrode was maintained at 70 % after 14 days of continuous use (Sakamoto et al., 2015).

This enzymatic biofuel cell was then integrated with our previously developed BioCapacitor to power various systems (Sode et al., 2016).

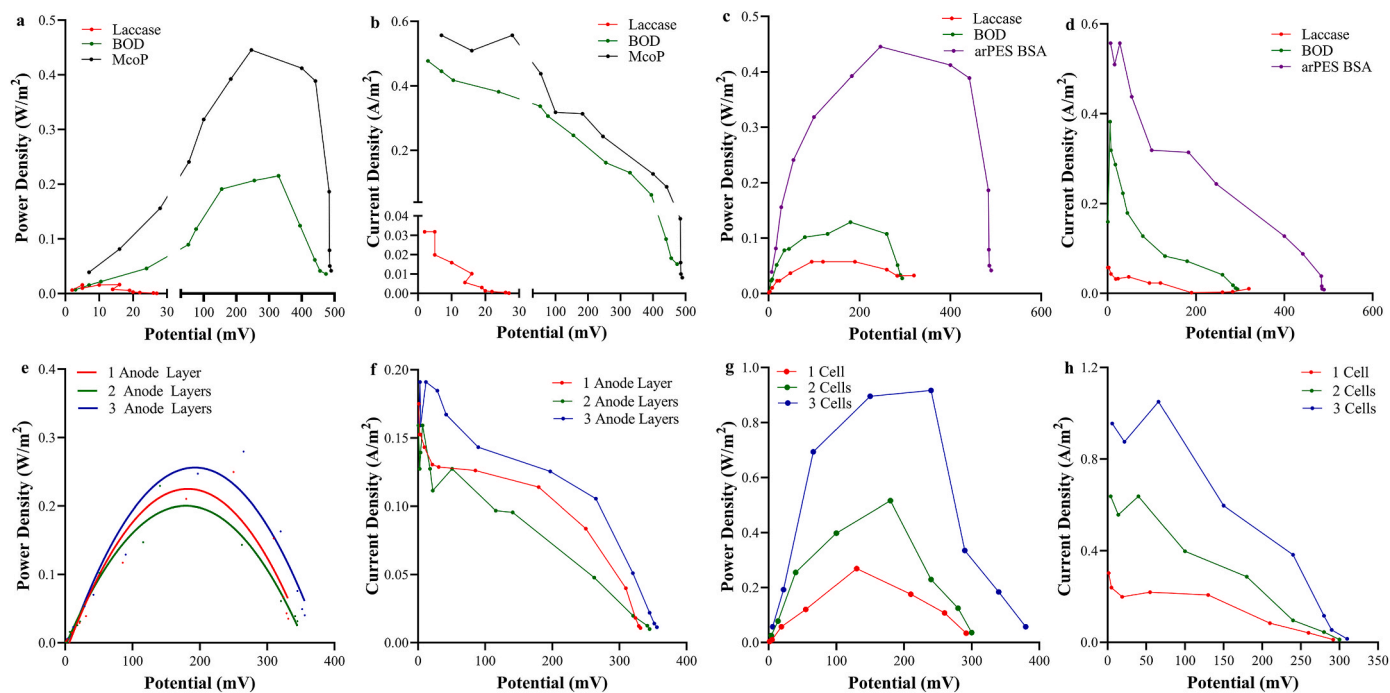


Fig. 2. (a–b) Power and current densities of anodes immobilized with various multicopper oxidases, paired with an arPES-BSA cathode. (c–d) Power and current densities of different cathodes paired with an McoP anode. (e–f) Characterization of the influence of the number of layers deposited on the anodic electrode. (g–h) Characterization of biofuel cells stacked in series and parallel, using 1 to 3 cells.

Past work from our group has already showcased the Bio Capacitor's capability to power systems such as actuators and microprocessors (Hanashi et al., 2014; Lee et al., 2017). Fig. 3 shows the enhanced performance achieved by shifting from GDEs to TCP electrodes. As demonstrated in Fig. 3a and b, a marked increase in both peak power and current output is observed upon this transition—GDE ($0.26 \text{ W/m}^2 \pm 0.02 \text{ W/m}^2$, $0.64 \text{ A/m}^2 \pm 0.04 \text{ A/m}^2$) and TCP ($0.85 \text{ W/m}^2 \pm 0.05 \text{ W/m}^2$, $0.89 \text{ A/m}^2 \pm 0.07 \text{ A/m}^2$). The intrinsic properties of the TCP electrodes, particularly its augmented surface area, are pivotal to this amplification, highlighting the importance of electrode material choice in fabricating biofuel cells. Using TCP electrodes has led to substantial advancements in power generation capabilities. To demonstrate this, we leveraged our previously utilized charge pump circuit to repeatedly charge a $47 \mu\text{F}$ capacitor (Fig. 3c) from a cold start and a $470 \mu\text{F}$ (average charge/discharge time of $\sim 23 \text{ s}$ across 10 cycles) capacitor (Fig. 3d). The generated power was able to accomplish approximately 35% efficiency as defined in Figs. 3 and 7 for the AD5090 specification sheet (Datasheet revision c), using a $V_{\text{in}} = 0.2 \text{ V}$, and an absolute current of $10 \mu\text{A}$ which is attainable based on our power curves shown in Fig. 3b.

The interest in alternative power sources for wearable and implantable devices has surged over the past decade. Conventional batteries, with their environmental waste, incompatibility with the human body, and finite lifespan, have inherently limited the development of implantable systems. Enzyme biofuel cells have emerged as a promising alternative, spurring research on developing modular enzyme biofuel cells for metabolite detection, powering low-energy Bluetooth devices, and even creating entirely self-powered systems. Several groups have developed enzymatic fuel cells utilizing glucose and lactate as fuels, harnessing enzymes to convert these fuels into useable power. Bollella et al. developed an enzymatic biofuel cell by immobilizing cellobiose dehydrogenase from *Corynascus thermophilus* on the anode, while the cathode employed *Trametes hirsuta* laccase (Bollella et al., 2018). This cell utilized glucose and oxygen as the anodic and cathodic fuels, respectively, achieving a power density of $1.57 \mu\text{W/cm}^2$ with just $100 \mu\text{M}$ of glucose. Rewatkar et al. conceived a paper-based enzymatic fuel cell using glucose oxidase as the anodic enzyme paired with a

mediator, and laccase as the cathodic enzyme. In various configurations, this setup yielded a power density of $46.4 \mu\text{W/cm}^2$ at an open circuit potential of 0.8 V (Rewatkar et al., 2020). Both these works are stellar examples of enzymatic biofuel cells which can be leveraged to power wearable systems. However, these designs still grapple with power limitations due to diffusion when put into practice. Our proposed model addresses these issues by embedding the fuel directly within the anode's matrix, whereas the cathode relies upon ambient oxygen which is readily available. This enables ease in miniaturization, and integration, as the system can be fabricated in a similar manner to oxygen type zinc oxide coin cells.

4. Conclusion

The work provided outlines the development of an enzyme fuel cell using multicopper oxidase as an anodic enzyme, which derives power without relying on substrate diffusion from the bulk environment. This innovative design paves the way for more comprehensive, closed enzyme fuel systems, termed as a BioBattery. In such systems, both the enzyme and fuel are encapsulated on the anode, while the cathode might utilize ambient electron acceptors like oxygen, which is abundant in nearly all bodily compartments. BioBattery not only integrates the anodic substrate directly, giving it a battery-like structure, but also pairs with our BioCapacitor to achieve higher voltages, broadening its potential uses. This work showcases the characterization of a system using several enzymes that oxidize phenolic compounds, achieved through the vapor deposition of glutaraldehyde, to power our previously developed BioCapacitor. The system consistently charged a $470 \mu\text{F}$ capacitor in under 25 s , enabling the powering of other modular systems.

CRedit authorship contribution statement

Kartheek Batchu: Writing – review & editing, Writing – original draft, Methodology, Investigation, Data curation, Conceptualization. **David Probst:** Writing – review & editing, Writing – original draft, Methodology, Investigation, Formal analysis, Conceptualization.

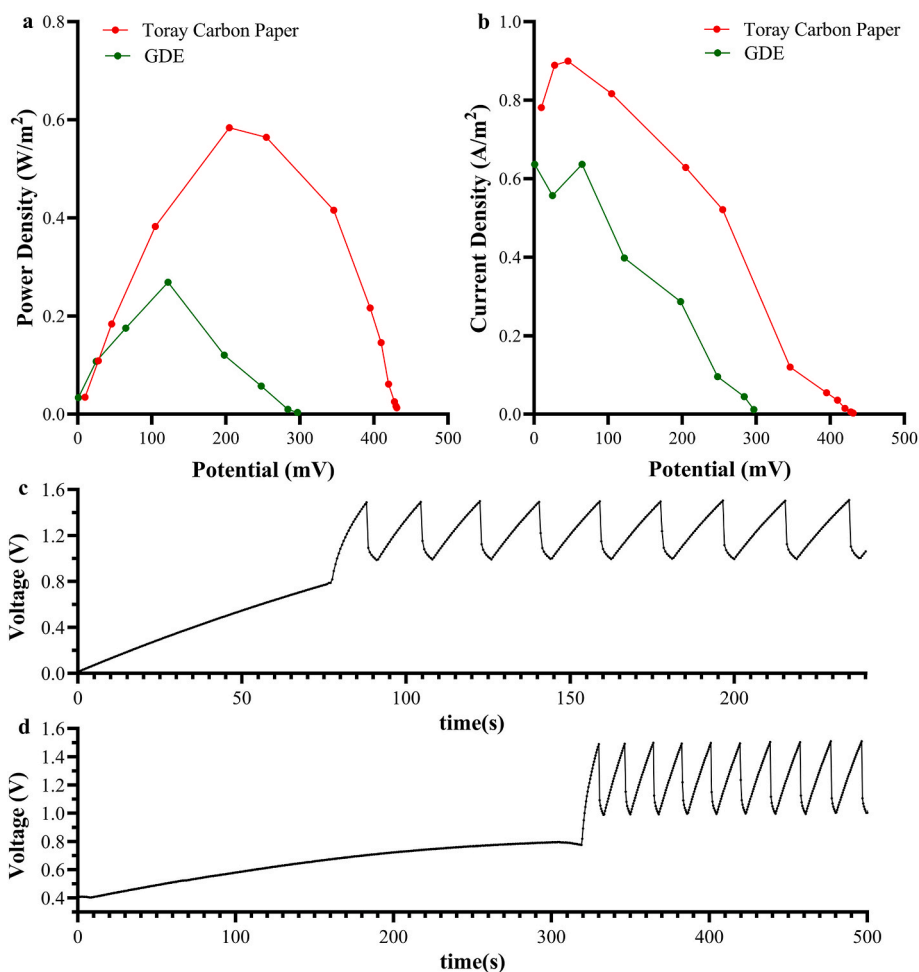


Fig. 3. (a-b) Comparative analysis of power and current output from BioBatteries using GDEs and TCP electrodes. Panels (c) and (d) depict successful charge/discharge cycles of capacitors connected to a charge pump circuit from a cold start, utilizing BioBatteries with TCP anodes and cathodes. Specifically, panel (c) shows cycles for a 47 μF capacitor from a cold start, while panel (d) demonstrates cycles for a 470 μF capacitor.

Takenori Satomura: Writing – review & editing, Writing – original draft, Supervision, Methodology. **Koji Sode:** Writing – review & editing, Writing – original draft, Supervision, Resources, Project administration, Funding acquisition, Conceptualization.

Declaration of competing interest

The authors declare the following financial interests/personal relationships which may be considered as potential competing interests:

Koji Sode reports financial support was provided by National Science Foundation. Koji Sode reports financial support was provided by Air Force Research Laboratory. Koji Sode reports financial support was provided by University of North Carolina at Chapel Hill and NC State University Joint Department of Biomedical Engineering. Koji Sode has patent #U.S. Provisional Patent Application No. 63/505,267 pending to the University of North Carolina at Chapel Hill. David Probst has patent #U.S. Provisional Patent Application No. 63/505,267 pending to the University of North Carolina at Chapel Hill. Kartheek Bachu has patent #U.S. Provisional Patent Application No. 63/505,267 pending to the University of North Carolina at Chapel Hill. Takenori Satomura has patent #U.S. Provisional Patent Application No. 63/505,267 pending to the University of North Carolina at Chapel Hill. The authors declare no other competing interests. If there are other authors, they declare that they have no known competing financial interests or personal relationships that could have appeared to influence the work reported in this paper.

Data availability

Data will be made available on request.

Acknowledgements

This research was done in collaboration with the National Science Foundation (EEC1160483) through the NSF Nanosystems Engineering Research Center (NERC) for Advanced Self-Powered Systems of Integrated Sensors and Technologies (ASSIST). This research was also financially supported by the Joint Program of Biomedical Engineering at University of North Carolina and Chapel Hill. This material is also based on research sponsored by Air Force Research Laboratory under agreement number FA8650-18-2-5402. The U.S. Government is authorized to reproduce and distribute reprints for Government purposes notwithstanding any copyright notation thereon. The views and conclusions contained herein are those of the authors and should not be interpreted as necessarily representing the official policies or endorsements, either expressed or implied, of Air Force Research Laboratory (AFRL) or the U. S. Government (clearance information: originator reference number: RX24-0168, case reviewer: Keith Klug, and case number: AFRL-2024-0861). Fig. 1 was created with BioRender.com.

Appendix A. Supplementary data

Supplementary data to this article can be found online at <https://doi.org/10.1016/j.bios.2024.116092>.

[org/10.1016/j.bios.2024.116092](https://doi.org/10.1016/j.bios.2024.116092).

Abbreviations

PES	Phenazine ethosulfate
arPES	amine-reactive PES
BSA	bovine serum albumin
McoP	multicopper oxidase from <i>Pyrobaculum aerophilum</i>
BOD	bilirubin oxidase
GDE	gold disk electrode
TCP	toray carbon paper
KB	Ketjen black
PPB	potassium phosphate buffer
OCP	open-circuit potential

References

- Barelli, L., Bidini, G., Pelosi, D., Sisani, E., 2021. Enzymatic biofuel cells: a review on flow designs. *Energies* 14, 910. <https://doi.org/10.3390/en14040910>.
- Bolletta, P., Fusco, G., Stevar, D., Gorton, L., Ludwig, R., Ma, S., Boer, H., Koivula, A., Tortolini, C., Favero, G., Antiochia, R., Mazzei, F., 2018. A glucose/oxygen enzymatic fuel cell based on gold nanoparticles modified graphene screen-printed electrode. Proof-of-Concept in human saliva. *Sensor. Actuator. B Chem.* 256, 921–930. <https://doi.org/10.1016/j.snb.2017.10.025>.
- Calabrese Barton, S., Gallaway, J., Atanassov, P., 2004. Enzymatic biofuel cells for implantable and microscale devices. *Chem. Rev.* 104, 4867–4886. <https://doi.org/10.1021/cr020719k>.
- Datasheet revision c; <https://www.analog.com/en/products/adp5090.html#product-overview>.
- Gough, D.A., Leyboldt, J.K., Armour, J.C., 1982. Erogress toward a potentially implantable, enzyme-based glucose sensor. *Diabetes Care* 5, 190. <https://doi.org/10.2337/diacare.5.3.190>.
- Hanashi, T., Yamazaki, T., Tsugawa, W., Ikebukuro, K., Sode, K., 2011. BioRadioTransmitter: a self-powered wireless glucose-sensing system. *J. Diabetes Sci. Technol.* 5, 1030–1035. <https://doi.org/10.1177/193229681100500502>.
- Hanashi, T., Yamazaki, T., Tanaka, H., Ikebukuro, K., Tsugawa, W., Sode, K., 2014. The development of an autonomous self-powered bio-sensing actuator. *Sensor. Actuator. B Chem.* 196, 429–433. <https://doi.org/10.1016/j.snb.2014.01.117>.
- Harris, A., 2007. *Power Management for Processor Core Voltage Requirements*. Texas Instruments Incorporated.
- Heikenfeld, J., Jajack, A., Feldman, B., Granger, S.W., Gaitonde, S., Begtrup, G., Katchman, B.A., 2019. Accessing analytes in biofluids for peripheral biochemical monitoring. *Nat. Biotechnol.* 37, 407–419. <https://doi.org/10.1038/s41587-019-0040-3>.
- Heller, A., 2004. Miniature biofuel cells. *Phys. Chem. Chem. Phys.* 6, 209. <https://doi.org/10.1039/b313149a>.
- Jeeran, I., Sempionatto, J.R., Wang, J., 2020. On-body bioelectronics: wearable biofuel cells for bioenergy harvesting and self-powered biosensing. *Adv. Funct. Mater.* 30, 1906243 <https://doi.org/10.1002/adfm.201906243>.
- Karim, A., N, Yang, H., 2021. Mini-review: recent Technologies of electrode and system in the enzymatic biofuel cell (EBFC). *Appl. Sci.* 11, 5197. <https://doi.org/10.3390/app11115197>.
- Kumar, A., Sharma, S., Pandey, L.M., Chandra, P., 2018. Nanoengineered material based biosensing electrodes for enzymatic biofuel cells applications. *Materials Science for Energy Technologies* 1, 38–48. <https://doi.org/10.1016/j.mset.2018.04.001>.
- Lee, I., Okuda-Shimazaki, J., Tsugawa, W., Ikebukuro, K., Sode, K., 2021. A self-powered glucose sensor based on BioCapacitor principle with micro-sized enzyme anode employing direct electron transfer type FADGDH. *JPhys Energy* 3, 034009. <https://doi.org/10.1088/2515-7655/abec32>.
- Lee, I., Sode, T., Loew, N., Tsugawa, W., Lowe, R.C., Sode, K., 2017. Continuous operation of an ultra-low-power microcontroller using glucose as the sole energy source. *Biosens. Bioelectron.* 93, 335–339. <https://doi.org/10.1016/j.bios.2016.09.095>.
- Migneault, I., Dartiguenave, C., Bertrand, M.J., Waldron, K.C., 2004. Glutaraldehyde: behavior in aqueous solution, reaction with proteins, and application to enzyme crosslinking. *Biotechniques* 37, 790–802. <https://doi.org/10.2144/04375RV01>.
- Pucino, V., Bombardieri, M., Pitzalis, C., Mauro, C., 2017. Lactate at the crossroads of metabolism, inflammation, and autoimmunity. *Eur. J. Immunol.* 47, 14–21. <https://doi.org/10.1002/eji.201646477>.
- Rewatkar, P., U. S, J., Goel, S., 2020. Optimized shelf-stacked paper origami-based glucose biofuel cell with immobilized enzymes and a mediator. *ACS Sustainable Chem. Eng.* 8, 12313–12320. <https://doi.org/10.1021/acssuschemeng.0c04752>.
- Satomura, T., Hirano, T., Inagaki, K., Horinaga, K., Takamura, E., Sakamoto, H., Ohshida, T., Ohshima, T., Sakuraba, H., Suye, S., 2021. Activity enhancement of multicopper oxidase from a hyperthermophile via directed evolution, and its application as the element of a high performance biocathode. *J. Biotechnol.* 325, 226–232. <https://doi.org/10.1016/j.jbiotec.2020.10.019>.
- Sharma, A., Singh, G., Arya, S.K., 2021. Biofuel cell nanodevices. *Int. J. Hydrogen Energy* 46, 3270–3288. <https://doi.org/10.1016/j.ijhydene.2020.02.164>.
- Slate, A.J., Whitehead, K.A., Brownson, D.A.C., Banks, C.E., 2019. Microbial fuel cells: an overview of current technology. *Renew. Sustain. Energy Rev.* 101, 60–81. <https://doi.org/10.1016/j.rser.2018.09.044>.
- Sode, K., Yamazaki, T., Lee, I., Hanashi, T., Tsugawa, W., 2016. BioCapacitor: a novel principle for biosensors. *Biosens. Bioelectron.* 76, 20–28. <https://doi.org/10.1016/j.bios.2015.07.065>.
- Xiao, X., Xia, H., Wu, R., Bai, L., Yan, L., Magner, E., Cosnier, S., Lojou, E., Zhu, Z., Liu, A., 2019. Tackling the challenges of enzymatic (Bio)Fuel cells. *Chem. Rev.* 119, 9509–9558. <https://doi.org/10.1021/acs.chemrev.9b00115>.